Visualization of localized store-operated calcium entry in mouse astrocytes. Close proximity to the endoplasmic reticulum

Vera A. Golovina

Department of Physiology, University of Maryland School of Medicine, Baltimore, MD 21201, USA

Unloading of endoplasmic reticulum (ER) Ca^{2+} stores activates influx of extracellular Ca^{2+} through 'store-operated' Ca^{2+} channels (SOCs) in the plasma membrane (PM) of most cells, including astrocytes. A key unresolved issue concerning SOC function is their spatial relationship to ER Ca^{2+} stores. Here, using high resolution imaging with the membrane-associated Ca^{2+} indicator, FFP-18, it is shown that store-operated Ca^{2+} entry (SOCE) in primary cultured mouse cortical astrocytes occurs at plasma membrane–ER junctions. In the absence of extracellular Ca^{2+}, depletion of ER Ca^{2+} stores using cyclopiazonic acid, an ER Ca^{2+}-ATPase inhibitor, and caffeine transiently increases the sub-plasma-membrane Ca^{2+} concentration ($[Ca^{2+}]_{SPM}$) within a restricted space between the plasma membrane and adjacent ER. Restoration of extracellular Ca^{2+} causes localized Ca^{2+} influx that first increases $[Ca^{2+}]_{SPM}$ in the same restricted regions and then, with a delay, in ER-free regions. Antisense knockdown of the TRPC1 gene, proposed to encode endogenous SOCs, markedly reduces SOCE measured with Fura-2. High resolution immunocytochemistry with anti-TRPC1 antibody reveals that these TRPC-encoded SOCs are confined to the PM microdomains adjacent to the underlying 'junctional' ER. Thus, Ca^{2+} entry through TRPC-encoded SOCs is closely linked, not only functionally, but also structurally, to the ER Ca^{2+} stores.

(Resubmitted 11 February 2005; accepted 23 February 2005; first published online 24 February 2005)
Corresponding author V. A. Golovina: Department of Physiology, University of Maryland School of Medicine, 685 W. Baltimore Street, Baltimore, MD 21201, USA. Email: vgolovin@umaryland.edu

Astrocytes play a complex role in the CNS: they not only provide structural and metabolic support for neurones, but also actively participate in intracellular signalling (Araque *et al.* 1999). The dynamic bi-directional form of communication between astrocytes and neurones depends mainly on Ca^{2+} oscillations and waves (Pasti *et al.* 1997) supported by localized Ca^{2+} release from the endoplasmic reticulum (ER) and extracellular Ca^{2+} entry (Yagodin *et al.* 1995). The spatial and temporal regulation of Ca^{2+} signalling in astrocytes is therefore critical (Blaustein & Golovina, 2001). Recent findings indicate that Ca^{2+} entry through 'store-operated' Ca^{2+} channels (SOCs) in the plasma membrane (PM) appears to be essential to sustain such Ca^{2+} oscillations (Pizzo *et al.* 2001; Sergeeva *et al.* 2003). This store-depletion-activated Ca^{2+} influx, known as 'capacitative' or store-operated Ca^{2+} entry (SOCE), is the primary mode of regulated Ca^{2+} entry in electrically non-excitable cells (Putney, 1990; Berridge, 1995).

Substantial evidence indicates that mammalian SOCs are formed by members of a family of seven proteins (TRPC1–TRPC7) that are homologous to the *Drosophila* transient receptor potential (trp) protein involved in phototransduction (Harteneck *et al.* 2000; Clapham *et al.* 2001; Montell, 2001). In particular, four of these proteins, TRPC1, TRPC2, TRPC4 and TRPC5, may form subunits of the endogenous SOCs activated solely by Ca^{2+} store depletion, while TRPC3, TRPC6 and TRPC7 can be activated by inositol trisphosphate (IP_3) and/or diacylglycerol and may not be store dependent (Harteneck *et al.* 2000). The involvement of TRPCs in SOCE in astrocytes, however, is not clear (Pizzo *et al.* 2001; Grimaldi *et al.* 2003).

Two general mechanisms for opening SOCs have been proposed (Irvine, 1990; Berridge, 1995). One involves a diffusible messenger, presumed to be released from the ER during Ca^{2+} store depletion, that might open SOCs (Randriamampita & Tsien, 1993; Trepakova *et al.* 2000). Alternatively, direct interaction between the ER IP_3 receptor (IP_3R) Ca^{2+} release channels and plasma membrane SOCs, as a result of store depletion, may trigger SOC opening (Irvine, 1990; Berridge, 1995; Boulay *et al.* 1999). Such interaction is supported by coimmunoprecipitation of TRPCs and IP_3R (Boulay *et al.* 1999). The structural integrity of plasma membrane–'junctional' ER units and the spatial

 DOI: 10.1113/jphysiol.2005.085035

relationship between SOCs and the ER Ca^{2+} stores may play an important role in regulating Ca^{2+} influx. Both SOCE models imply that the PM microdomains containing SOCs are situated in close proximity to the ER. Direct information is, however, lacking about the precise location of SOCs relative to the ER and whether TRPCs contribute to SOCE in astrocytes. These issues are addressed in the present study.

To directly visualize SOCE high spatial resolution imaging with the membrane-associated Ca^{2+} indicator FFP-18 was employed. FFP-18 is a lipophilic analogue of Fura-2 (Vorndran *et al.* 1995), which is incorporated into the inner face of the PM (Davies & Hallett, 1996, 1998). FFP-18 has been successfully used to monitor rapid changes in the sub-plasma-membrane Ca^{2+} concentration ($[Ca^{2+}]_{SPM}$) in a variety of cell types (Etter *et al.* 1994, 1996; Graier *et al.* 1998; Davies & Hallett, 1998; Chadborn *et al.* 2002). Using FFP-18 imaging and high resolution immunocytochemistry with anti-TRPC antibody, it is demonstrated here that SOCE signals and encoded by TRPC genes SOCs in cortical astrocytes localize to the PM microdomains adjacent to the underlying 'junctional' ER.

Methods

Astrocyte cultures

All experiments were carried out according to the guidelines of the Institutional Animal Care and Use Committee of the University of Maryland School of Medicine. Primary cultured cortical astrocytes were prepared from the brains of 17- to 18-day-old C57BL/6J mouse embryos, as described previously (Golovina *et al.* 2003); mice were killed by cervical dislocation and fetuses were removed. Cerebral cortices from four to eight fetal mice were separated from the meninges and the hippocampus. The cortices were placed in culture medium (Dulbecco's modified Eagle's medium (DMEM/F12 with 10% fetal bovine serum (FBS), penicillin G (50 U ml^{-1}), and streptomycin (50 $\mu g\,ml^{-1}$)) and were mechanically dissociated by sequential passage through 80 μm and 10 μm nylon mesh to give a single cell suspension. The dissociated cells were plated on either poly-L-lysine-coated 25 mm glass coverslips for use in fluorescence microscopy experiments or on coverslips with a lettered grid for counting. The cells were characterized as protoplasmic (type 1) astroglial cells (Bambrick *et al.* 1996). Experiments were performed on subconfluent cultures on days 8–14 *in vitro*.

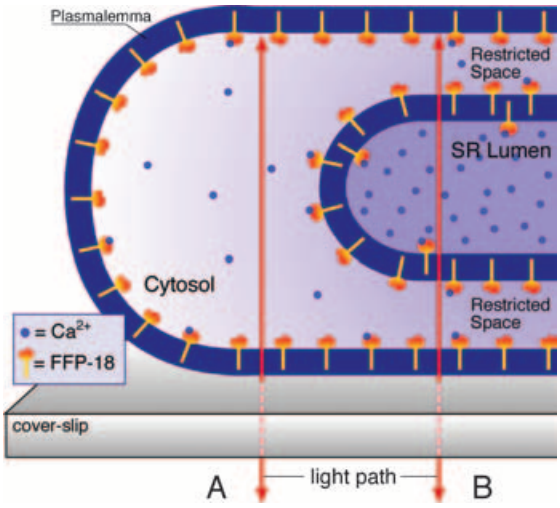

Figure 1. Illustration of the method used to image sub-PM microdomains in cells loaded with FFP-18
Diagram shows a cross-section (*X–Z* plane) of a small region at the periphery of an FFP-18-loaded cell. There are two wide-field fluorescence light paths. Light in path 'A' is emitted from dye in the PM facing the cytosol at the bottom and top. This dye signals changes in the $[Ca^{2+}]$ near the PM. Light in path 'B' is emitted from dye in the PM and ER membranes facing the tiny PM–ER cytosolic spaces at the bottom and at the top. Localization of dye molecules in the ER membrane facing the ER lumen is negligible, as confirmed by the relatively uniform resting FFP-18 ratio image shown in Fig. 2*Da*.

Calcium imaging

Cytosolic Ca^{2+} concentration ($[Ca^{2+}]_{cyt}$) and $[Ca^{2+}]_{SPM}$ were measured with, respectively, Fura-2 and Fura-piperazine-$C_{12}H_{25}$ (FFP-18; TEFLabs, Austin, TX, USA) by using digital imaging. Details of the fluorescence imaging and analysis techniques are published (Golovina & Blaustein, 2000). FFP-18 consists of a Ca^{2+}-sensitive fluorescent Fura group linked via a piperazine group to an acyl chain. The 12-carbon acyl chain is believed to insert into the lipid bilayer while the charged piperazine moiety floats on the surface of the membrane, in a manner similar to a phospholipid head group (Vorndran *et al.* 1995; Chadborn *et al.* 2002). FFP-18 is used to monitor rapid, large (up to 4 μM; K_d for $Ca^{2+} = 0.4\ \mu$M) changes in $[Ca^{2+}]_{SPM}$ (Davies & Hallett, 1996; Graier *et al.* 1998). FFP-18 was used here to measure store-operated Ca^{2+} translocation across the PM.

Astrocytes grown on coverslips were loaded with Fura-2 (30 min) or FFP-18 (2 h) by incubating them in culture medium (20–22°C, 5% CO_2–95% O_2) containing 3.3 μM Fura-2-AM or 5 μM FFP-18-AM. Exogenously added FFP-18-AM initially incorporates into the outer leaflet of the PM, but as molecules reorient to face the inner surface by slow 'flip-flop' diffusion, cytosolic esterases cleave the ester groups. The Ca^{2+}-sensitive FFP-18 acid is generated on the inner face and is unable to diffuse back (Davies *et al.* 1997; Davies & Hallett, 1998).

Figure 1 diagrams the possible distribution of FFP-18 used to image sub-PM microdomains in astrocytes loaded with this dye. Some FFP-18 inserts into the ER membrane mainly facing the PM–ER cytosolic space. The amount of FFP-18 facing the ER lumen appears to be negligible (see Results and Discussion). The FFP-18 signal was

unaffected by application of 2 mM Ni^{2+} (not shown), which quenches the FFP-18 fluorescence on the external face of the PM (Davies & Hallett, 1996). This confirms that the FFP-18 Ca^{2+}-sensitive head group was facing into the cell, monitoring cytosolic rather than extracellular [Ca^{2+}]. Because the process of 'flip-flop' diffusion is slow compared to diffusion of Fura-2-AM (Davies *et al.* 1997), time of cell loading with FFP-18-AM is longer than with Fura-2-AM.

After loading with either dye, the coverslips were transferred to a tissue chamber mounted on a microscope stage, where cells were superfused for 15–20 min (35–36°C) with standard physiological salt solution to wash away extracellular dye. The physiological salt solution, PSS, contained (mM): 140 NaCl, 5.9 KCl, 1.2 NaH_2PO_4, 5 $NaHCO_3$, 1.4 $MgCl_2$, 1.8 $CaCl_2$, 11.5 glucose, and 10 Hepes (pH 7.4). Cells were studied for 40–60 min while being continuously superfused with PSS (35°C).

The imaging system was designed around a Zeiss Axiovert 100 microscope (Carl Zeiss, Thornwood, NY, USA) optimized for UV transmission. The dye-loaded cells were illuminated with a diffraction grating-based system (Polychrome II, Applied Scientific Instruments, Eugene, OR, USA) (Golovina & Blaustein, 2000). Fluorescence images were recorded by using a General III ultrablue intensified charge-coupled device camera (Stanford Photonics, Palo Alto, CA, USA). Image acquisition and analysis were performed with a MetaFluor/MetaMorph Imaging System (Universal Imaging, West Chester, PA, USA). Cultured astrocytes are particularly well suited for such wide-field fluorescence microscopy because they are very thin (Z axis $\leq 1\,\mu$m); thus the ER can be resolved in the X–Y plane. The limit of Z-axis resolution with confocal laser scanning microscopy is $\sim 0.7\,\mu$m (Miriel *et al.* 1999). Therefore, confocal microscopy cannot resolve intracellular structures in the Z-axis in cells with a Z-axis dimension $\leq 1\,\mu$m.

$[Ca^{2+}]_{cyt}$ was calculated by determining the ratio of Fura-2 fluorescence excited at 380 and 360 nm as described previously (Golovina & Blaustein, 2000). FFP-18 fluorescence data are presented as 340 nm/380 nm wavelength ratios (510 nm emission).

Immunofluorescence microscopy

Astrocytes were immunolabelled, as described by Luther & Bloch (1989). Briefly, cells were fixed in cyclohexylamine–formaldehyde fixative consisting of 0.45% (w/v) formaldehyde, 75 mM cyclohexylamine, 75 mM NaCl, 10 mM EGTA, 10 mM $MgCl_2$ and 10 mM PIPES. After fixation, the cells were permeabilized in fixative containing 0.5% polyoxyethylene 20 cetyl ether (Brij 58), and were then incubated (4–17 h) in antibody buffer containing antibodies against the various transporters. For surface staining, non-permeabilized cells were blocked with 10% goat serum, and incubated with primary antibody (Antoniotti *et al.* 2002). The following antibodies were used: rabbit polyclonal anti-TRPC1, anti-TRPC4 (Allomone Laboratories, Israel); rabbit polyclonal anti-TRPC1 (gift of Dr G. Krapivinsky, Harvard Medical School, Boston, MA, USA); rabbit polyclonal anti-α_{1D} subunit of L-type voltage-gated Ca^{2+} channels (Allomone Laboratories); monoclonal anti-SERCA2 (Affinity BioReagents, Golden, CO, USA); rabbit polyclonal anti-SERCA2b (gift of Dr F. Wuytak, Katholieke University, Leuven, Belgium); rabbit polyclonal anti-PM Ca^{2+}-ATPase (gift of Dr E. Carafoli, University of Padova, Italy); rabbit polyclonal anti-IP_3R type 1 (gift of Dr R. J. Wojcikiewicz, State University of New York, Syracuse Health Science Center, Syracuse, NY, USA). FITC-labelled donkey antimouse IgG or Cy3-conjugated donkey antirabbit IgG (Jackson ImmunoResearch, West Grove, PA, USA) were used to visualize the primary antibodies. The fluorescence from the secondary antibody in the absence of primary antibody (positive control) did not exceed 2–3% of the fluorescence in the presence of antiserum.

To identify ER in living and fixed astrocytes, cells were treated (5 min) with 200 ng ml^{-1} 3,3′-dihexyloxacarbocyanine, $DiOC_6(3)$ (DiOC) (Golovina & Blaustein, 2000), or 1 μM ER-Tracker (Molecular Probes, Eugene, OR, USA).

Immunoprecipitation

Cultured astrocytes were rinsed, scraped into phosphate-buffered saline (PBS) and subjected to centrifugation for 15 min at 15 000 *g* and 4°C. The cell pellet was resuspended in ice-cold extraction buffer (1% IGEPAL CA-630 (Sigma), 150 mM NaCl, 2 mM EDTA, 10 mM sodium azide, 20 mM Tris-HCl (pH 7.4) and protease inhibitor mixture tablets (Roche Diagnostics, Germany)), followed by 10 passages each through 10- and 25-gauge needles and incubated for 1 h at 4°C. The lysate was centrifuged for 20 min at 27 000 *g* and 4°C. The supernatant (detergent extract or 'Homogenate') was stored at −80°C and used for immunoprecipitation and immunoblotting. The protein concentration was determined with the bicinchoninic acid assay (Bio-Rad), with bovine serum albumin as a standard. Appropriate polyclonal antibodies were incubated with $\sim 2 \times 10^7$ (60 μl) washed magnetic beads (Dynabeads M-450, coated with M-280 sheep antirabbit IgG, Dynal Biotech, Lake Success, NY, USA) overnight at 4°C on a rotator, as described by Lencesova *et al.* (2004). As negative controls, the coated beads were incubated with rabbit γ-globulin (Jackson ImmunoResearch, West Grove, PA, USA) for polyclonal antibodies raised in rabbits. The beads, with antibody attached, were washed (twice, 200 μl) with PBS. Proteins were immunoprecipitated from 1 mg of

detergent-extracted total protein by incubation for 4 h at 4°C with antibody-bound beads. Following incubation, bead complexes were washed (4 times 400 μl) with PTA (145 mM NaCl, 10 mM NaH_2PO_4, 10 mM sodium azide, and 0.5% Tween 20, pH 7.0). Immunoprecipitated proteins were then extracted with 50 μl of 2 × Laemmli sample buffer (Bio-Rad) and boiled for 5 min.

Western immunoblot analysis

Membrane proteins were separated by 7.5% SDS-PAGE as described by Golovina *et al.* (2003) and transferred electrophoretically to a nitrocellulose membrane (Amersham BioSciences). The membranes were blocked with 5% non-fat dry milk in Tris-buffered saline containing 0.1% Tween 20, incubated overnight at 4°C with appropriate primary antibody. Following washing, membranes were incubated with antirabbit horseradish peroxidase-conjugated IgG for 1 h at room temperature. The immune complexes on the membranes were detected with an enhanced chemiluminescence detection system (ECL Plus; Amersham BioSciences).

Antisense oligonucleotides

Next Generation™ antisense oligonucleotides (AS-oligos) were synthesized by Sequitur, Inc. (Natick, MA, USA). AS-oligos were directed at the TRPC1 coding sequences (AUAGUCACCCUUGUCGCACGCCAGC). Oligos with the same base composition, but with a scrambled sequence (CCACCUGAGUUCACCACGUCACUGG) controlled for non-specific or toxic effects of the oligos. The oligonucleotides were transfected into cells by Lipid 2012-G (Sequitur). Astrocytes were divided into three groups: (i) the antisense group was exposed to the AS-oligos; (ii) one control group was exposed to the scrambled (nonsense, NS) oligos; and (iii) the second control group was grown without oligos. For each treatment, the cells were first rinsed with Opti-MEM, after which the oligos were added to the cells. Following 16–24 h incubation, the medium was aspirated and replaced with growth medium without oligos for 48–60 h before Ca^{2+} measurement or immunocytochemistry was performed.

Statistical analysis

The numerical data presented in Results are the means ± S.E.M. from n single cells (one value per cell). Immunofluorescence labelling experiments were repeated at least four times. The number of different animals and different litters are also presented, where appropriate. Data from four to five litters were obtained for most protocols and were consistent from litter to litter. Statistical significance was determined using Student's t test and ANOVA.

Results

Store-operated Ca^{2+} influx colocalizes to the ER

When astrocytes are loaded with FFP-18, the hydrophobic analogue of Fura-2 (Etter *et al.* 1994; Davies & Hallett, 1996), much of the fluorescence signal comes from the inner surface of the PM and reflects $[Ca^{2+}]$ in that vicinity, i.e. $[Ca^{2+}]_{SPM}$ (Fig. 2). FFP-18 also inserts into the ER membrane, mainly facing the PM–ER cytosolic space (Fig. 1). There appears to be little or no contamination of the sub-PM signal with a signal from the lumen of the ER because the resting FFP-18 ratio image is relatively uniform (Fig. 2*Da*). Identification of the ER was confirmed at the end of each experiment by staining with DiOC (Fig. 2*C* and *F*).

Figure 2*B* shows the time course of changes in the FFP-18 ratio in an area overlying the ER (red) and in an ER-free region (blue), in response to the application of cyclopiazonic acid (CPA, an ER Ca^{2+} pump blocker) and caffeine (CAF). First, the Ca^{2+} stores were depleted in the absence of extracellular Ca^{2+}. Then, following store depletion, when changes in the $[Ca^{2+}]_{SPM}$ signal were no longer observed (~15 min), Ca^{2+} was added back and the rise in $[Ca^{2+}]_{SPM}$ due to SOCE was measured. To eliminate the contribution of Ca^{2+}-induced Ca^{2+} release (CICR) to the SOCE-evoked rise in $[Ca^{2+}]_{SPM}$, the solutions contained 1 μM ryanodine (RY). RY at this concentration locks the CICR channels in an open, low-conductance state (Smith *et al.* 1988); this promotes depletion of the CAF/RY-sensitive store by CAF (Golovina & Blaustein, 2000). The rise in $[Ca^{2+}]_{SPM}$ due to SOCE starts in the PM regions overlying the ER (Fig. 2*D*c, *E* and *G*); it is followed with a delay by Ca^{2+} increases in ER-free regions, as a result of Ca^{2+} diffusion. Note that the sites of SOCE (Figs 2*E* and *G*) colocalize with the sites of CPA + CAF-induced ER Ca^{2+} release (Fig. 2*E*), indicating their close association. The rates of Ca^{2+} diffusion from the sites of Ca^{2+} release and SOCE are comparable (5.5 ± 0.8 and 6.1 ± 1.2 μm s^{-1}, respectively; $n = 12$ cells). These rates are, however, lower than velocity of agonist (ATP)-induced Ca^{2+} waves in cultured astrocytes (17 ± 6 μm s^{-1}; $n = 58$ cells), comparable to published data for spread of Ca^{2+} waves (19 ± 9 μm s^{-1}; Cornell-Bell *et al.* 1990). This 3-fold difference in velocity may be explained by regenerative Ca^{2+} release along the length of the cell (Yagodin *et al.* 1995). SOCE can be heterogeneous. For example, in the area overlying the element of ER indicated by the lower arrowhead, the SOCE signal was larger than in the adjacent area (upper arrowhead). This is likely to be the consequence of a high density of SOC expression in these PM

microdomains and restricted Ca^{2+} diffusion in the tiny volume of cytosol located between the 'junctional' ER and the PM (Blaustein & Golovina, 2001). Modulation of PM Ca^{2+}-ATPase activity by local Ca^{2+} microdomains near SOCs (Bautista & Lewis, 2004) and/or regional differences in Ca^{2+} binding proteins might also contribute to local gradients of $[Ca^{2+}]_{SPM}$ in the regions overlying the ER (Fig. 2*D*).

The sites of SOCE signal initiation were compared with localization of Ca^{2+} influx through L-type voltage-gated Ca^{2+} channels ('contrast control'; Fig. 3). In marked contrast to the SOCE signal, 50 mM K^+-induced Ca^{2+} influx, which is blocked by dihydropyridines (not shown), and thus mediated by L-type Ca^{2+} channels, is uniform in all regions of the PM (Fig. 3*B–D*). To increase voltage-activated Ca^{2+} influx, high K^+ was applied with a Ca^{2+} channel agonist, BayK 8644 (10 μM) (MacVicar *et al.* 1991). The rate of high K^+-induced rise in $[Ca^{2+}]_{SPM}$ is 4- to 5-fold higher (Fig. 3*B* and *C* inset) than that due to SOCE (Fig. 2*B* inset, and *G*). This is likely the consequence of a higher density and/or larger conductance of L-type Ca^{2+} channels than SOCs (Parekh & Penner, 1997).

Inhibition of TRPC1 expression with antisense oligos reduces SOCE

Molecular identification of SOCs in astrocytes is essential for studying functional and spatial expression of SOCE. Figure 4 shows that mouse cortical astrocytes express TRPC1, which is an obligatory component of endogenous SOCs in a variety of cell types (Liu *et al.* 2000; Harteneck *et al.* 2000; Xu & Beech, 2001).

To determine whether TRPC1 is involved in SOCE in astrocytes, an antisense strategy was employed. Selective

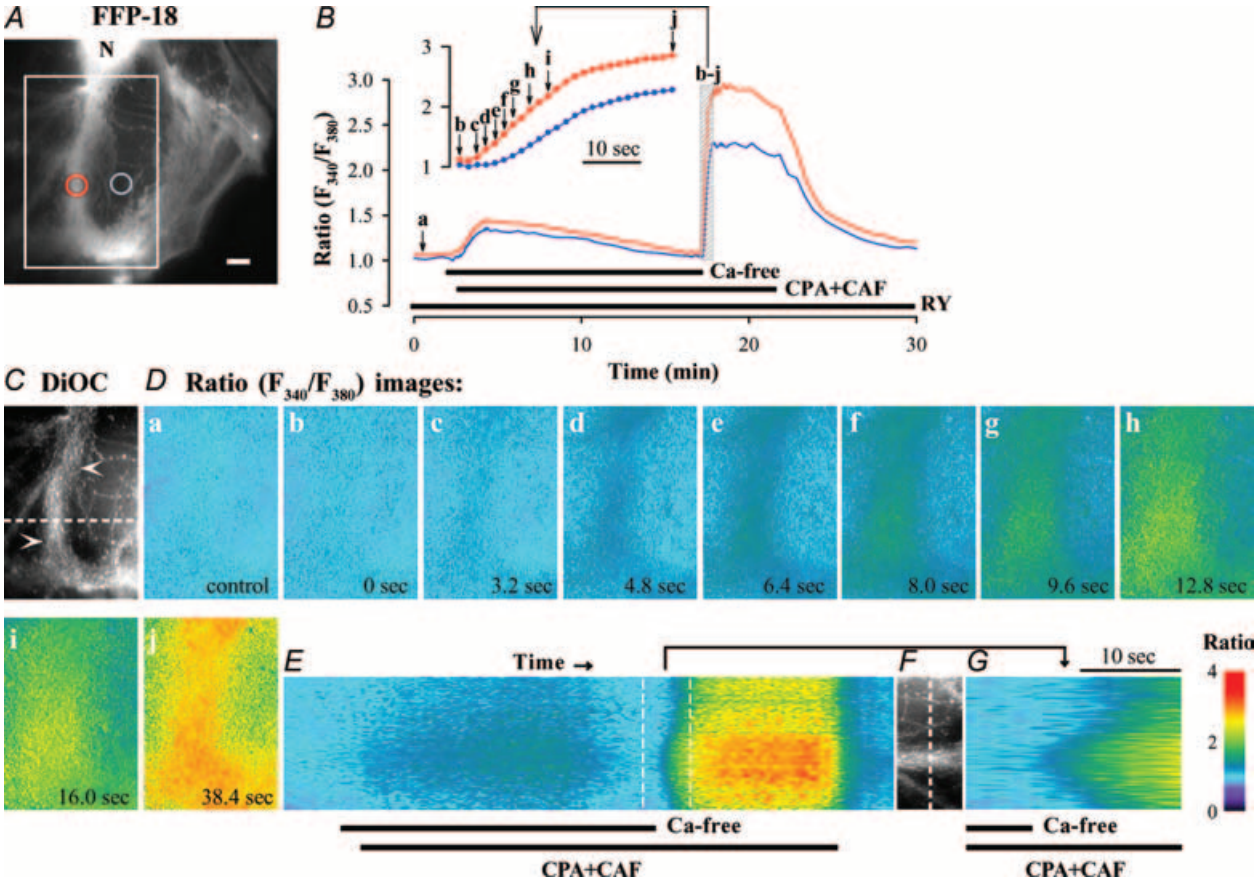

Figure 2. SOCE-induced local $[Ca^{2+}]_{SPM}$ signal in an astrocyte
A, FFP-18 (F_{360}) image of a portion of cell. To better visualize the ER, the image contrast was increased so that the ER appears to contain much more dye than is actually the case. N, nucleus. Scale bar = 25 μm. *B*, time course of ratio (F_{340}/F_{380}) signal in regions outlined in *A* (red and blue); times of treatment with CPA (10 μM) + CAF (10 mM) and Ca^{2+}-free solution are indicated. RY (1 μM) was applied 10 min before the traces shown and was maintained throughout the experiment. Inset shows the early rising phase of the F_{340}/F_{380} ratio after Ca^{2+} restoration. *C*, DiOC image of the boxed portion of *A*. Arrowheads point to ER (including mitochondria). Most mitochondria, which are brightly stained by DiOC, appeared to lie on the ER. *D*, ratio (F_{340}/F_{380}) images (*a–j*) captured at the times indicated in *B*. *E*, linescan of CPA + CAF-induced changes in ratio (F_{340}/F_{380}), shown in *B*, along the white dotted line in *C* and *F*. The time scale is variable. *G*, linescan with high time scale resolution (from the boxed portion in *E*). Scale bar = 10 s. Comparable results were obtained in 12 other cells.

inhibition of TRPC1 protein expression, using AS-oligos targeted to the TRPC1 gene (Fig. 4*A* and *B*), significantly attenuated the SOC-mediated rise of $[Ca^{2+}]_{cyt}$, measured with Fura-2 (311 ± 18 *versus* 1090 ± 48 nM in cells treated with NS-oligos) (Fig. 4*C* and *D*). The cells in all three groups retained normal morphology, but astrocyte proliferation was inhibited in the AS-oligos treated group (Fig. 4*F*). TRPC1 knockout cells were distinguished from non-transfected cells by staining with anti-TRPC1 antibody (Fig. 4*Eb*) immediately after physiological experiments with Fura-2. The cells were then also labelled with the nucleic acid stain 4′,6′-diamidino-2-phenylindole (DAPI, 5 μM) to estimate the total cell number in the field (Fig. 4*Ec*). Figure 4 shows that 6 of the 8 cells treated with AS-oligos did not express detectable TRPC1 (Fig. 4*Ea* and *b*) and exhibited significantly attenuated SOCE (Fig. 4*C*). Some nuclei also appear to be slightly fluorescent (Fig. 4*Eb*) due to non-specific labelling by the secondary antibody (see Methods). All untreated (control) cells expressed TRPC1 (not shown). These results strongly suggest that TRPC1 is an essential component of the endogenous SOCs that mediate SOCE in mouse cortical astrocytes. Moreover, the results support the view that TRPC1 gene expression regulates astrocyte proliferation by modulating SOCE activity (Golovina *et al.* 2001).

TRPC proteins localize to PM microdomains adjacent to underlying ER

High resolution immunocytochemistry was used to elucidate the relationship between the sites of SOCE signal initiation (Fig. 2) and the specific location of TRPC proteins in the PM. Figure 5 shows the distribution of endogenous TRPC proteins in intact (non-transfected) astrocytes. The low magnification image demonstrates that TRPC1 label is distributed in a distinct reticular pattern (Fig. 5*A*) that parallels the organization of the underlying ER-Tracker-stained ER (Fig. 5*B*). This reticular pattern indicates that clusters of TRPC1 in the PM are organized around the underlying ER.

High power images of a portion of another astrocyte show that the reticular TRPC1 labelling pattern (Fig. 5*Da*) is remarkably similar to the pattern observed with antibodies directed against the ER Ca^{2+} pump, SERCA2 (Fig. 5*Db*) or with ER-Tracker (Fig. 5*Dc*). The confinement of TRPC1 to PM microdomains that overlie ER in astrocytes is consistent with the proposed role of this protein as an essential component of SOC. The identical TRPC1 and SERCA distribution is likely to have functional significance, as SOCE is a major pathway involved in refilling ER Ca^{2+} stores: SOCE-regulated ER stores communicate with the PM to modulate Ca^{2+} entry as a function of ER Ca^{2+} concentration ($[Ca^{2+}]_{ER}$) (Hofer *et al.* 1998). Notably, reactivity was not detected in the PM in the absence of the primary antibody (not shown) or when anti-TRPC1 antibody was first incubated with the peptide (Fig. 5*C*).

TRPC channels are assembled as homo- or hetero-TRPC tetramers (Hoffman *et al.* 2002). In particular, TRPC1 has the unique ability to form channel complexes together with TRPC4 and TRPC5 (Hoffman *et al.* 2002). As shown in Fig. 5*E*, TRPC4 protein also localizes to PM microdomains adjacent to underlying ER. To confirm that the reticular pattern of TRPC labelling is not an

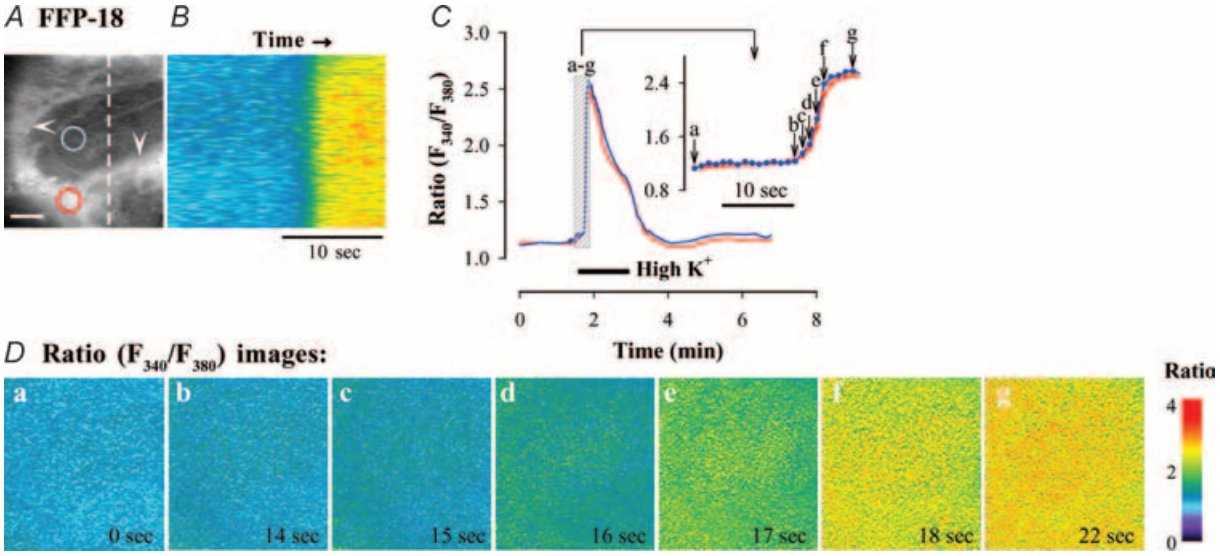

Figure 3. High K^+-induced $[Ca^{2+}]_{SPM}$ signal in an astrocyte
A, FFP-18 (F_{360}) image of a small portion of cell; scale bar = 25 μm. *B*, linescan of high K^+-induced changes in ratio along the white dotted line in *A*. *C*, time courses of ratio (F_{340}/F_{380}) signal in regions outlined in *A* (red and blue); time of treatment with 50 mM KCl is indicated. Inset shows the early rising phase of the F_{340}/F_{380} ratio. *D*, ratio (F_{340}/F_{380}) images captured at the times indicated in *C* inset. Comparable results were obtained in eight other cells.

artifact, its distribution is compared with that of the PM Ca^{2+} pump, which is distributed uniformly over the cell surface (Juhaszova *et al.* 1997). TRPC labelling is also compared with distribution of L-type voltage-gated Ca^{2+} channels (α_{1D} subunit), which are expressed in astrocytes (Latour *et al.* 2003). In contrast to the TRPC proteins, PM Ca^{2+} pump and L-type Ca^{2+} channel labelling are clearly different from the reticular pattern of SERCA2 (Fig. 5*Fa* and *b*) or ER labelling (Fig. 5*Ga* and *b*).

TRPC1 is a PM protein spanning the membrane with an extracellular domain (Xu & Beech, 2001). To confirm the PM localization of endogenous TRPC protein in astrocytes immunicytochemical experiments were repeated on non-permeabilized cells by using TRPC1 antibody targeted to peptide predicted to contribute to the outer vestibule of the pore, between the fifth and the sixth transmembrane segments (Antoniotti *et al.* 2002). Figure 5*H* shows a reticular pattern of TRPC1 PM staining, but no SERCA2 (i.e. ER) labelling in non-permeabilized triple-stained cell. Background fluorescence (Fig. 5*Hb*) is non-specific from the secondary antibody and did not exceed 2–3% of the fluorescence of permeabilized cells in the presence of SERCA2b antibody (Fig. 5*Db*). ER-Tracker (Fig. 5*Hc*) which also stains non-permeabilized cells, has a distribution similar to TRPC1 (Fig. 5*Ha*). These data are consistent with the FFP-18 results demonstrating a distinct reticular pattern of distribution of SOCE signal (Fig. 2).

The colocalization of TRPC-encoded SOCs with the ER at PM–ER junctions in astrocytes suggests that there is a special structural relationship between TRPCs and elements of the ER. To confirm this, immunoprecipitates (IPs) of endogenously expressed TRPC1 were prepared from detergent-solubilized extracts of mouse astrocyte membranes. Immunoblots were performed on these IPs to determine whether TRPC1 forms a complex with ER Ca^{2+}

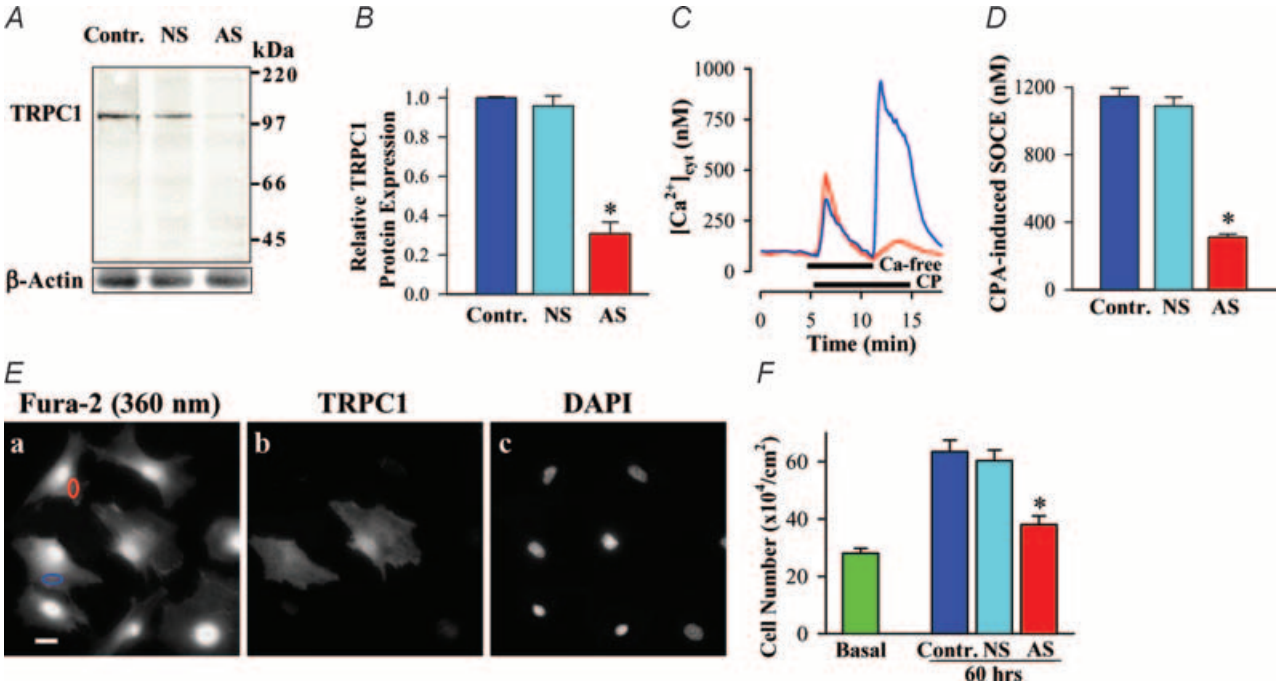

Figure 4. Effect of antisense oligos for the TRPC1 gene on TRPC1 protein expression, SOCE and astrocyte proliferation

A, Western blot of TRPC1 expression in control cells (no oligos), and in astrocytes treated with NS- or AS-oligos. Proteins (10 μg/lane) were separated on 7.5% polyacrylamine gel, blotted, and probed with specific anti-TRPC1 antibody. Blots were later incubated with anti-β-actin antibodies to verify uniform protein loading. *B*, data are normalized to the amount of β-actin and are expressed as means ± S.E.M. from 15 fetuses (3 litters). *$P < 0.001$ *versus* NS. *C*, representative records showing time course of $[Ca^{2+}]_{cyt}$ changes in cells with disrupted TRPC1 expression (red) and in non-transfected cells (blue). Red and blue records correspond to spatially averaged changes in $[Ca^{2+}]_{cyt}$ within the small red and blue ovals, respectively, in the fura-2 fluorescence images in *Ea*. CPA (10 μM) was applied to the cells in the absence and presence of extracellular Ca^{2+}, as indicated. *D*, summarized data showing the amplitude of SOCE induced by CPA. Data are means ± S.E.M. ($n = 58$ cells; 10 coverslips). *$P < 0.001$ *versus* NS. Each bar shows data from 9 to 12 fetuses from 3 litters (3–4 fetuses/litter). *E*, Fura-2 fluorescence (F_{360}) image (*a*) showing the cells in which $[Ca^{2+}]_{cyt}$ was measured (scale bar = 25 μm). Following the Ca^{2+} imaging experiment, the same cells were immunocytochemically stained for TRPC1 (*b*) and then labelled with DAPI (*c*). Two DAPI-labelled cells were TRPC1 positive, indicating they were not transfected with AS-oligos; six cells were non-fluorescent indicating inhibition of TRPC1 expression (*b*). *F*, cell numbers were determined before (Basal) and after incubating 60 h in control growth medium (10% FBS) (Contr) or media containing NS- or AS-oligos. Data are means ± S.E.M. of 4 experiments/litters (53 coverslips). *$P < 0.001$ *versus* NS.

transporters and receptors. Co-immunoprecipitation data revealed that TRPC1 in mouse cortical astrocytes, indeed, interacts not only with IP_3R type 1, but also with SERCA2b (Fig. 6*A*). For controls, the Dynabeads were coated with non-specific rabbit γ-globulin (γ-Gl) for polyclonal antibodies. No TRPC1 bound to these beads. The data were confirmed by complementary (converse) experiments: IP with an antibody rose against SERCA2b or IP_3R-1 coimmunoprecipitated TRPC1 (Fig. 6*B*). TRPC1-reactive band was not found in SERCA2b IP when anti-TRPC1 antibody was preincubated with antigen peptide (not shown). This demonstrates that the coimmunoprecipitated immunoreactive band in the SERCA2b IP is TRPC1. The results indicate that there is a physical association between TRPC channels and ER Ca^{2+} stores.

Discussion

The experiments described here demonstrate that direct visualization of localized SOCE signals is possible by using wide-field imaging with the near-membrane Ca^{2+} indicator, FFP-18. The data indicate that SOCE in primary cultured mouse cortical astrocytes occurs at PM–ER junctions. This conclusion is confirmed by immunocytochemical observations and by coimmunoprecipitation data showing that PM microdomains adjacent to the underlying ER contain TRPC channel proteins which are components of SOCs.

Association between the PM and ER

SOCE is a mechanism that links $[Ca^{2+}]_{ER}$ to PM Ca^{2+} permeability and serves as an important pathway to refill

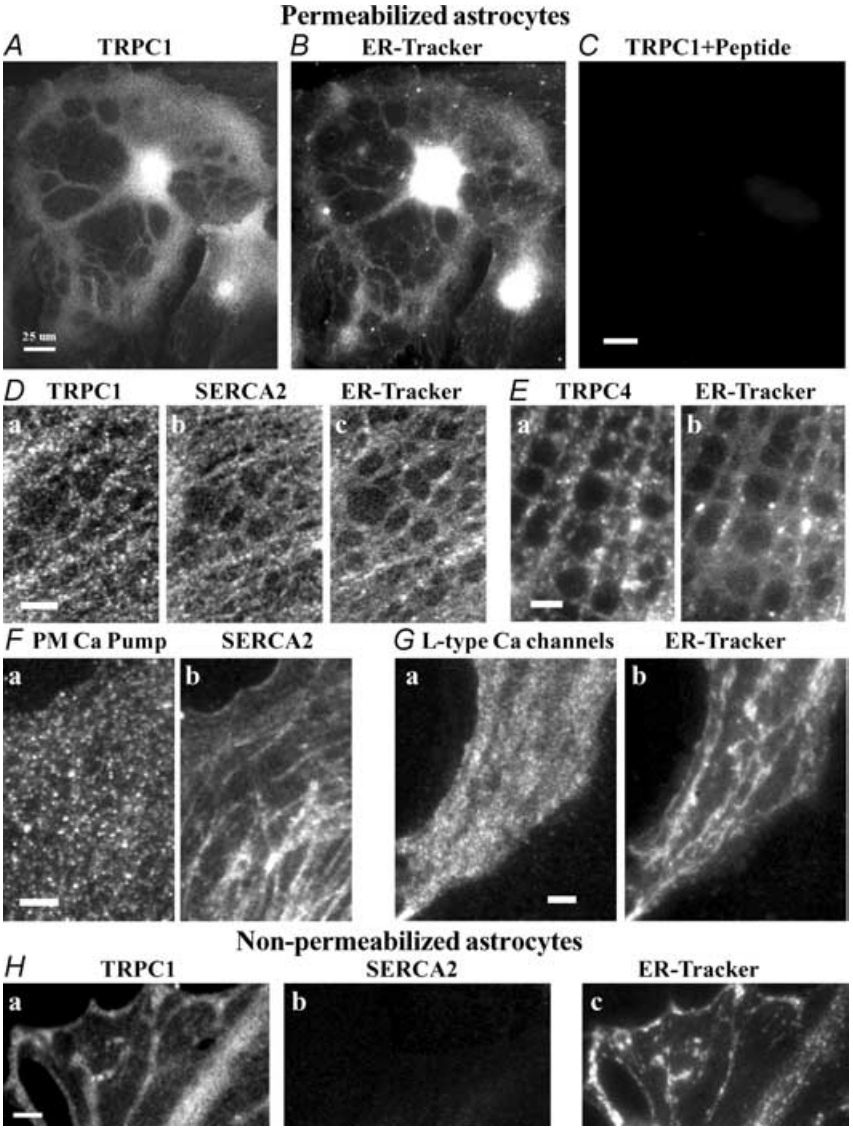

Figure 5. Immunofluorescent localization of TRPC proteins in astrocytes
A and *B*, low magnification images of cells crossreacted with anti-TRPC1 antibody (*A*); ER-Tracker was later used to stain the ER (*B*). *C*, fluorescence detected when the primary antibody was preincubated with TRPC1 peptide. *D*, high magnification images of a portion of an astrocyte triple labelled with anti-TRPC1 antibody (*a*), anti-SERCA-2 antibody (*b*), and ER-Tracker (*c*). All three labels show similar reticular distributions. *E*, images of a portion of another astrocyte double labelled with anti-TRPC4 antibodies (*a*), and ER-Tracker (*b*). *F*, high power images of a portion of astrocyte double labelled with anti-PM Ca^{2+}-ATPase (*a*) and anti-SERCA-2 antibodies (*b*). *G*, images of a portion of astrocyte double labelled with anti-L-type Ca^{2+} channel antibody (*a*) and ER-Tracker (*b*). *H*, images of a portion of a non-permeabilized astrocyte triple labelled with anti-TRPC1 antibody (*a*), anti-SERCA-2 antibody (*b*), and ER-Tracker (*c*). Scale bars = 25 μm (*A* and *C*), 5 μm (*Da*, *Ea* and *Fa*), and 10 μm (*Ga* and *Ha*). Similar results were obtained in 18 cells (*A* and *B*), 53 cells (*D*), 37 cells (*E*), 14 cells (*F*), 11 cells (*G*), and 15 cells (*H*) from 16 fetuses (4 litters).

intracellular Ca^{2+} stores. Therefore one may conjecture that specificity of such intimate functional interaction between ER Ca^{2+} stores and PM SOCs is determined by their spatial proximity (Berridge, 1995; Peterson & Berridge, 1996; Jaconi *et al.* 1997; Putney, 1999). Indeed, in many cell types, the peripheral ER membrane frequently comes within 8–20 nm of the PM, with which it appears to form 'junctions' with periodic structures spanning the gap (Henkart *et al.* 1976; Watanabe & Burnstock, 1976; Somlyo & Franzini-Armstrong, 1985). In neurones, PM–junctional ER units appear structurally similar to the PM–sarcoplasmic reticulum (SR) junctions in the triads and diads of skeletal and cardiac muscle (Henkart *et al.* 1976; Blaustein & Golovina, 2001). Van Breemen *et al.* (1995) suggest that there is a second space between the PM and SR that is narrow and restricted, but not 'junctional'. Diffusion of ions from such PM–superficial ER compartments to 'bulk' cytosol must be markedly restricted (Van Breemen *et al.* 1995; Delmas & Brown, 2002). Therefore Ca^{2+} entering the cells is directly accumulated by the peripheral ER without altering bulk $[Ca^{2+}]_{cyt}$ (Van Breemen *et al.* 1995; Blaustein & Golovina, 2001; Flemming *et al.* 2002). This may explain why Ca^{2+} influx fails to induce contraction in some smooth muscle when SR Ca^{2+} stores are depleted by SERCA inhibitors (Flemming *et al.* 2002). In cells undergoing continuous Ca^{2+} oscillations, the entry of Ca^{2+} to replenish repeatedly releasing Ca^{2+} stores is critical (Venkatachalam *et al.* 2002).

SOCE occurs at PM–ER junctions

Close association between some ER Ca^{2+} release sites and SOCE has been reported in *Xenopus* oocytes. For instance, agonist-evoked ER Ca^{2+} release in restricted regions stimulates Ca^{2+} entry-activated chloride currents only in those same regions (Peterson & Berridge, 1996). Also, following centrifugation of *Xenopus* oocytes to redistribute their organelles, thapsigargin-induced Ca^{2+} release localizes to the ER layer and Ca^{2+} enters in adjacent PM regions (Jaconi *et al.* 1997). The sites of SOCE, however, have not been visualized in astrocytes or any other type of cells with intact intracellular morphology.

Localization of Ca^{2+} entry in the vicinity of SOCs requires high spatial resolution. The distance between the PM and the junctional ER (~20 nm) is less than the optical resolution of light microscopes. Therefore, these tiny sub-PM compartments have not been imaged by confocal, deconvolution or two-photon microscopy, all of which have Z-axis resolution $\leq 0.7\ \mu$m (Juhaszova & Blaustein, 1997; Miriel *et al.* 1999). Measurement of $[Ca^{2+}]_{SPM}$ with total internal reflection fluorescence (TIRF) is also limited because Z-axis resolution is about one-fifth the effective thickness of confocal or two-photon fluorescence, i.e. ~150–200 nm (Axelrod, 2001). Thus, measurements of Ca^{2+} in the restricted space between the PM and junctional ER (~20 nm) also cannot be resolved by TIRF. Therefore alternative methods are required. To monitor $[Ca^{2+}]_{SPM}$ membrane-tethered Ca^{2+} indicators, such as FFP-18, have been developed (Etter *et al.* 1994; Vorndran *et al.* 1995; Lloyd *et al.* 1995). Several reports demonstrate that this indicator does, indeed, monitor changes in $[Ca^{2+}]_{SPM}$ rather than the bulk $[Ca^{2+}]_{cyt}$ (Davies *et al.* 1997; Paltauf-Doburzynska *et al.* 1998; Chadborn *et al.* 2002).

This study reveals that SOCE starts at PM regions overlying the ER. The Ca^{2+} then spreads relatively slowly to nearby cytosol as long as SERCA is inhibited (Fig. 2).

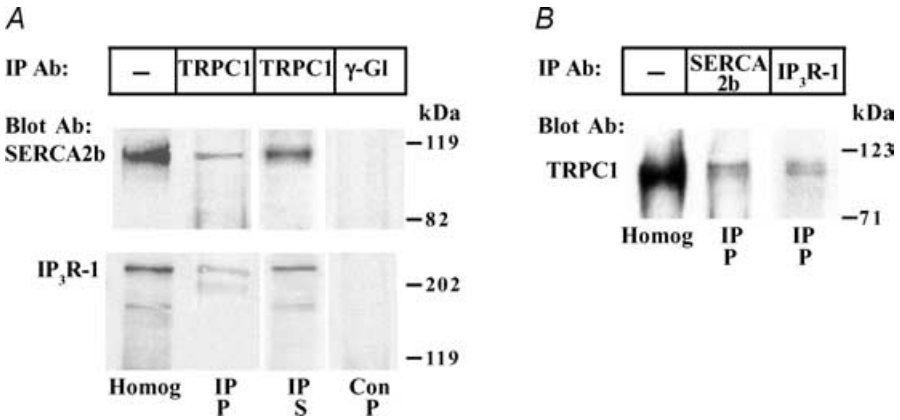

Figure 6. Coimmunoprecipitation of endogenous TRPC1 with SERCA2b and IP_3R-1 in mouse cortical astrocytes

A, TRPC1 immunoprecipitate (IP) was generated and probed with anti-SERCA2b and anti-IP_3R type 1 antibodies. Control beads were prepared with rabbit γ-globulin (γ-Gl). Gels were loaded with homogenate (Homog, 1st lane; 2 μg protein for SERCA2b and 10 μg protein for IP_3R-1), IP pellet (IP P, 2nd lane; 10 μl of IP protein solution for all co-IPs); post-IP supernatant (IP S, 3rd lane, same volume as 1st lane) and pellet eluted from γ-globulin-IP beads (Con P, 4th lane). *B*, SERCA2b and IP_3R-1 IPs probed with TRPC1 antibody. Reactivity to anti-TRPC1 was blocked by preincubating the antibody with the peptide (not shown). Molecular masses are indicated in kDa.

FFP-18 may also insert into the ER membrane, but mainly facing the PM–ER cytosolic space (Fig. 1). Localization of dye molecules in the ER membrane facing the ER lumen is negligible, as confirmed by the relatively uniform resting FFP-18 ratio image (Fig. 2*Da*). (FFP-18 in the ER membrane facing the lumen should be saturated with Ca^{2+} because $[Ca^{2+}]_{ER} > 150\ \mu M$ (Golovina & Blaustein, 1997), this is about 375 times larger than the FFP-18 K_d ($0.4\ \mu M$). This would give rise to a non-uniform resting FFP-18 ratio image, which was not observed. Furthermore, the expected decline in $[Ca^{2+}]_{ER}$ during store depletion cannot be confused with the rise in $[Ca^{2+}]_{SPM}$ caused by SOCE because the $[Ca^{2+}]$ signals from the ER and sub-PM space should move in *opposite* directions.) Furthermore, when the ER Ca^{2+} stores are unloaded for 15 min in Ca^{2+}-free media, the FFP-18 ratio (F_{340}/F_{380}) first increases, indicating a rise in $[Ca^{2+}]_{SPM}$, and then returns to the same initial level (Fig. 2*Da* and *b*), i.e. the FFP-18 signal does not reflect the expected changes in ER lumenal Ca^{2+}. Moreover, external Ca^{2+} was restored and SOCE was activated only when localized $[Ca^{2+}]_{SPM}$ changes following store depletion were no longer observed (Figs 2*B* and *E*). Particularly noteworthy is the fact that the sites of SOCE signal initiation (Fig. 2*G*) are remarkably different from the sites of Ca^{2+} influx through L-type voltage-gated Ca^{2+} channels, which are ubiquitously distributed in all regions of the PM (Fig. 3*B*). This approach permits the visualization of localized $[Ca^{2+}]_{SPM}$ changes even if the precise magnitude of SOCE-induced changes in $[Ca^{2+}]_{SPM}$ is more difficult to resolve. The data presented here indicate that SOCE has preferred access to the ER.

PM–ER compartments might include mitochondria (Dahl *et al.* 1965; Malli *et al.* 2003), which are able to buffer Ca^{2+} entering through both SOCs and voltage-gated Ca^{2+} channels (Parekh, 2003). Mitochondria can generate sustained sub-PM microdomains of low $[Ca^{2+}]$ and modulate SOCE by controlling its magnitude and duration (Malli *et al.* 2003; Parekh, 2003): this does not, however, alter the conclusion that SOCs are confined to PM–ER junction compartments. Mitochondrial buffering might contribute to the heterogeneity of localized SOCE signals in the regions overlying the ER (Fig. 2*D*). Further studies are required to determine the impact of mitochondrial Ca^{2+} signalling on localized SOCE in cortical astrocytes.

Endogenous TRPC1 is involved in SOCE in astrocytes

Mammalian SOCs are believed to consist of TRPC protein tetramers (Harteneck *et al.* 2000; Xu & Beech, 2001). The presence of TRPC proteins in astrocytes has previously been demonstrated (Pizzo *et al.* 2001; Grimaldi *et al.* 2003) although their involvement in SOCE is not clear. For instance, Pizzo and colleagues compared TRPC expression in rat cortical astrocytes and RBL-2H3 cells and did not find a simple correlation between the level of TRPC expression and the magnitude of SOCE. It is commonly believed that within the TRPC family TRPC1 is an obligatory component of endogenous SOCs in a variety of cell types (Harteneck *et al.* 2000). The present study, using antisense oligos, demonstrates that TRPC1 is also involved in SOCE in mouse cortical astrocytes. Cell transfection with antisense oligos targeted to the TRPC1 gene reduced, by ~70%, both expression of TRPC1 protein (Fig. 4*A* and *B*) and SOCE (Fig. 4*D*).

TRPC proteins localize to the PM microdomains adjacent to the underlying ER

The distribution of the TRPC proteins in the PM of astrocytes has not been previously described. Low-resolution immunocytochemical studies in other cells, however, indicate that endogenous TRPCs are not distributed uniformly. For example, in primary cultured human myometrial smooth muscle cells, TRPC1, TRPC3, TRPC4 and TRPC6 proteins appear to be distributed in a reticular fashion (Dalrymple *et al.* 2002). In a line of native cultured bovine aortic endothelial cells (BAE-1 cells), the TRPC1 labelling is also punctate (Antoniotti *et al.* 2002; Fig. 3*A*), suggesting that this protein is distributed in an organized manner in the PM. In the present study clear reticular patterns of PM distribution of TRPC proteins were demonstrated by using high spatial resolution immunocytochemistry on permeabilized as well as on non-permeabilized astrocytes. There is striking similarity in the distribution of TRPC proteins and ER labelling with SERCA2 or ER-tracker in both permeabilized (Fig. 5*D*) and non-permeabilized astrocytes (Fig. 5*Ha* and *c*); in contrast, no immunofluorescent SERCA2 labelling (i.e. ER) is observed in non-permeabilized cells (Fig. 5*Hb*). This observation demonstrates that TRPC proteins are present on the cell surface. The data confirm previous reports demonstrating PM localization of TRPC1 protein in native non-permeabilized vascular smooth muscle cells (Xu & Beech, 2001) and in endothelial cells (Antoniotti *et al.* 2002). The reticular pattern of PM localization of TRPC-encoded SOCs is consistent with the close proximity of the SOCE signals to the ER. This differs from the uniform distribution of L-type voltage-gated Ca^{2+} channels and high K^+-induced Ca^{2+} influx.

TRPC1 forms a Ca^{2+} signalling complex with ER Ca^{2+} transporters

Coimmunoprecipitation data indicate that, when TRPC proteins are transfected into heterologous cells, they interact with endogenous IP_3Rs (Boulay *et al.* 1999;

Kiselyov *et al.* 2000; Tang *et al.* 2001) or with RY receptors (Kiselyov *et al.* 2000). The present study demonstrates that endogenous TRPC1 in primary cultured astrocytes coimmunoprecipitates not only with IP_3Rs but also with SERCA2b (Fig. 6); this is consistent with the immunocytochemical data showing the structural relationship between the TRPC1 and SERCA2 (Fig. 5*D*). The data support the idea that PM microdomains containing TRPC channels form Ca^{2+} signalling complexes with adjacent ER Ca^{2+} transporters in astrocytes. PM microdomains containing TRPC channels might be linked to the underlying junctional ER by adaptor/scaffolding proteins (Yuan *et al.* 2003). In a recent study Treves *et al.* (2004) demonstrated that PM–ER compartments are stabilized by 'junctate', an integral Ca^{2+} binding protein of ER membrane, that forms a supramolecular complex with the IP_3R and the TRPC3 and modulates Ca^{2+} entry through receptor- and store-activated channels in T3-HEK293 cells.

In summary, this report directly demonstrates that TRPC-encoded SOCs in astrocytes, and the SOCE they mediate, are situated very close to the sub-PM ER. Such specialized distribution of PM SOCs, relative to the ER, facilitates functional, and possibly structural coupling of SOCs to the ER Ca^{2+} stores. In this way, the Ca^{2+} content of the ER can be regulated independently of changes in bulk cytoplasmic $[Ca^{2+}]$.

Numerous observations indicate that PM microdomains that overlie the closely apposed junctional ER compartments are functionally specialized because of their unique complements of ion transporters (Blaustein & Golovina, 2001; Lencesova *et al.* 2004). In astrocytes, for instance, these PM microdomains contain clusters of isoform-specific Na^+ pumps ($\alpha 2$) and Na^+–Ca^{2+} exchangers (Juhaszova *et al.* 1997). As shown here, these PM microdomains also contain TRPC-encoded SOCs. Thus, the PM–junctional ER complexes function as integrated units that regulate the initiation and spread of Ca^{2+} signals in astrocytes.

References

Antoniotti S, Lovisolo D, Fiorio PA & Munaron L (2002). Expression and functional role of TRPC1 channels in native endothelial cells. *FEBS Lett* **510**, 189–195.

Araque A, Parpura V, Sanzgiri RP & Haydon PG (1999). Tripartite synapses: glia, the unacknowledged partner. *Trends Neurosci* **22**, 208–215.

Axelrod D (2001). Selective imaging of surface fluorescence with very high aperture microscope objectives. *J Biomed Optics* **6**, 6–13.

Bambrick LL, de Grip A, Seenivasan V, Krueger BK & Yarovsky PJ (1996). Expression of glial antigens in mouse astrocytes: species differences and regulation in vitro. *J Neurosci Res* **46**, 305–315.

Bautista DM & Lewis RS (2004). Modulation of plasma membrane calcium-ATPase activity by local calcium microdomains near CRAC channels in human T cells. *J Physiol* **556**, 805–817.

Berridge MJ (1995). Capacitative calcium entry. *Biochem J* **312**, 1–11.

Blaustein MP & Golovina VA (2001). Structural complexity and functional diversity of endoplasmic reticulum Ca^{2+} stores. *Trends Neurosci* **24**, 602–608.

Boulay G, Brown DM, Qin N, Jiang M, Dietrich A, Zhu MX, Chen Z, Birnbaumer M, Mikoshiba K & Birmbaumer L (1999). Modulation of Ca^{2+} entry by polypeptides of the inositol 1,4,5-trisphosphate receptor (IP3R) that bind transient receptor potential (TRP): evidence for roles of TRP and IP3R in store depletion-activated Ca^{2+} entry. *Proc Natl Acad Sci U S A* **96**, 14955–14960.

Chadborn N, Eickholt B, Doherty P & Boisover S (2002). Direct measurement of local raised subplasmalemmal calcium concentrations in growth cones advancing on an N-cadherin substrate. *Eur J Neurosci* **15**, 1891–1898.

Clapham DE, Runnels LW & Strubing C (2001). The TRP ion channel family. *Nat Rev Neurosci* **2**, 387–396.

Cornell-Bell AH, Finkbeiner SM, Cooper MS & Smith SJ (1990). Glutamate induces calcium waves in cultural astrocytes: long-range glial signaling. *Science* **247**, 470–373.

Dahl E, Flora G & Nelson E (1965). Electron microscopic observations on normal human intracranial arteries. *Neurology* **15**, 120–140.

Dalrymple A, Slater DM, Beech D, Poston L & Tribe RM (2002). Molecular identification and localization of Trp homologues, putative calcium channels, in pregnant human uterus. *Mol Hum Reprod* **8**, 946–951.

Davies EV, Blanchfield H & Hallett MS (1997). Use of fluorescent dyes for measurement and localization of organelles associated with Ca^{2+} store release in human neutrophils. *Cell Biol Int* **21**, 655–663.

Davies EV & Hallett MS (1996). Near membrane Ca^{2+} changes resulting from store release in neutrophils: detection by FFP-18. *Cell Calcium* **19**, 355–362.

Davies EV & Hallett MS (1998). High micromolar Ca^{2+} beneath the plasma membrane in stimulated neutrophils. *Biochem Biophys Res Commun* **248**, 679–693.

Delmas P & Brown DA (2002). Junctional signaling microdomains: bridging the gap between the neuronal cell surface and Ca^{2+} stores. *Neuron* **36**, 787–790.

Etter EF, Kuhn MA & Fay FS (1994). Detection of changes in near-membrane Ca^{2+} concentration using a novel membrane-associated Ca^{2+} indicator. *J Biol Chem* **269**, 10141–10149.

Etter EF, Minta A, Poenie M & Fay FS (1996). Near-membrane $[Ca^{2+}]$ transients resolved using the Ca^{2+} indicator FFP18. *Proc Natl Acad Sci U S A* **93**, 5369–5373.

Flemming R, Cheong A, Dedman AM & Beech DJ (2002). Discrete store-operated calcium influx into an intracellular compartment in rabbit arteriolar smooth muscle. *J Physiol* **543**, 455–464.

Golovina VA & Blaustein MP (1997). Spatially and functionally distinct Ca^{2+} stores in sarcoplasmic and endoplasmic reticulum. *Science* **275**, 1643–1648.

Golovina VA & Blaustein MP (2000). Unloading and refilling of two classes of spatially resolved endoplasmic reticulum Ca^{2+} stores in astrocytes. *Glia* **31**, 15–28.

Golovina VA, Platoshyn O, Baley CL, Wang J, Limsuwan A, Sweeney M, Rubin LJ & Yuan JX-J (2001). Upregulated TRP and enhanced capacitative Ca^{2+} entry in human pulmonary artery myocytes during proliferation. *Am J Physiol* **280**, H746–H755.

Golovina VA, Song H, James PF, Lingrel JB & Blaustein MP (2003). Na^+ pump α_2-subunit expression modulates Ca^{2+} signaling. *Am J Physiol* **284**, C475–C486.

Graier WF, Paltauf-Doburzynska J, Hill BJF, Fleischhacker E, Hoebel BG, Kostner GM & Sturek M (1998). Submaximal stimulation of porcine endothelial cells causes focal Ca^{2+} elevation beneath the cell membrane. *J Physiol* **506**, 109–125.

Grimaldi M, Maratos M & Verma A (2003). Transient receptor potential channel activation causes a novel form of $[Ca^{2+}]_I$ oscillations and is not involved in capacitative Ca^{2+} entry in glial cells. *J Neurosci* **23**, 4737–4745.

Harteneck C, Plant TD & Schultz G (2000). From worm to man: three subfamilies of TRP channels. *Trends Neurosci* **23**, 159–166.

Henkart M, Landis DM & Reese TS (1976). Similarity of junctions between plasma membranes and endoplasmic reticulum in muscle and neurons. *J Cell Biol* **70**, 338–347.

Hofer AM, Fasolato C & Pozzan T (1998). Capacitative Ca^{2+} entry is closely linked to the filling state of internal Ca^{2+} stores: a study using simultaneous measurements of I_{CRAC} and intraluminal $[Ca^{2+}]$. *J Cell Biol* **140**, 325–334.

Hoffman T, Schaefer M, Schultz G & Gudermann T (2002). Subunit composition of mammalian transient receptor potential channels in living cells. *Proc Natl Acad Sci U S A* **99**, 7461–7466.

Irvine RF (1990). 'Quantal' Ca^{2+} release and the control of Ca^{2+} entry by inositol phosphates – a possible mechanism. *FEBS Lett* **263**, 5–9.

Jaconi M, Pyle J, Bortolon R, Ou J & Clapham D (1997). Calcium release and influx colocalize to the endoplasmic reticulum. *Curr Biol* **7**, 599–602.

Juhaszova M & Blaustein MP (1997). Na^+ pump low and high ouabain affinity α subunit isoforms are differently distributed in cells. *Proc Natl Acad Sci U S A* **94**, 1800–1805.

Juhaszova M, Shimizu H, Borin M, Yip RK, Santiago EM, Lindenmayer GE & Blaustein MP (1997). Localization of the Na^+/Ca^{2+} exchanger in vascular smooth muscle, and in neurons and astrocytes. *Ann NY Acad Sci* **779**, 318–335.

Kiselyov KI, Shin DM, Wang Y, Pessah IN, Allen PD & Muallem S (2000). Gating of store-operated channels by conformation coupling to ryanodine receptors. *Moll Cell* **6**, 421–431.

Latour I, Hamid J, Beedle AM, Zamponi GW & MacVicar BA (2003). Expression of voltage-gated Ca^{2+} channel subtypes in cultured astrocytes. *Glia* **41**, 347–353.

Lencesova L, O'Neill A, Resneck WG, Bloch RJ & Blaustein MP (2004). Plasma membrane-cytoskeleton-endoplasmic reticulum complexes in neurons and astrocytes. *J Biol Chem* **279**, 2885–2893.

Liu X, Wang W, Singh BB, Lockwich T, Jadlowiec J, O'Connell B, Wellner R, Zhu MX & Ambudkar IS (2000). TRPC1, a candidate protein for the store-operated Ca^{2+} influx mechanism in salivary gland cells. *J Biol Chem* **275**, 3403–3411.

Lloyd QP, Kuhns MA & Gay CV (1995). Characterization of calcium translocation across the plasma membrane of primary osteoblasts using a lipophilic calcium-sensitive fluorescent dye, calcium green C_{18}. *J Biol Chem* **270**, 22445–22451.

Luther PW & Bloch RJ (1989). Formaldehyde-amine fixatives for immunocytochemistry of cultured *Xenopus* myocytes. *J Histochem Cytochem* **37**, 75–82.

MacVicar BA, Hochman D, Delay KJ & Weiss S (1991). Modulation of intracellular Ca^{2+} in cultured astrocytes by influx through voltage-activated Ca^{2+} channels. *Glia* **4**, 448–455.

Malli R, Frieden M, Osibow K, Zoratti C, Mayer M, Demaurex N & Graier WF (2003). Sustain Ca^{2+} transfer across mitochondria is essential for mitochondrial Ca^{2+} buffering, store-operated Ca^{2+} entry, and Ca^{2+} store refilling. *J Biol Chem* **278**, 44769–44779.

Miriel VA, Mauban JRH, Blaustein MP & Wier WG (1999). Local and cellular Ca^{2+} transients in smooth muscle of pressurized rat resistance arteries during myogenic and agonist stimulation. *J Physiol* **518**, 815–824.

Montell C (2001). Physiology, phylogeny, and functions of the TRP superfamily of cation channels. *Science's STKE*, http://www.stke.org/cgi/content/full/OC_sigtrans; 2001.

Paltauf-Doburzynska J, Posch K, Paltauf G & Graier WF (1998). Stealth ryanodine-sensitive Ca^{2+} release contributes to activity of capacitative Ca^{2+} entry and nitric oxide synthase in bovine endothelial cells. *J Physiol* **513**, 369–379.

Parekh AB (2003). Store-operated Ca^{2+} entry: dynamic interplay between endoplasmic reticulum, mitochondria and plasma membrane. *J Physiol* **547**, 333–348.

Parekh AB & Penner R (1997). Store depletion and calcium influx. *Physiol Rev* **27**, 901–930.

Pasti L, Voltera A, Pozzan T & Carmignoto G (1997). Intracellular calcium oscillations in astrocytes, a highly plastic, bi-directional form of communication between neurons and astrocytes in situ. *J Neurosci* **17**, 7817–7830.

Peterson CCH & Berridge MJ (1996). Capacitative calcium entry is colocalised with calcium release in *Xenopus* oocytes: evidence against a highly diffusible calcium influx factor. *Pflugers Arch* **432**, 286–292.

Pizzo P, Burgo A, Pozzan T & Fasolato C (2001). Role of capacitative calcium entry on glutamate-induced calcium influx in type-1 rat cortical astrocytes. *J Neurochem* **89**, 98–109.

Putney JW Jr (1990). Capacitative calcium entry revisited. *Cell Calcium* **7**, 1–12.

Putney JW Jr (1999). "Kissin' cousins": intimate plasma membrane–ER interactions underlie capacitative calcium entry. *Cell* **99**, 5–8.

Randriamampita C & Tsien RY (1993). Emptying of intracellular calcium stores releases a novel small messenger that stimulates calcium influx. *Nature* **364**, 809–814.

Sergeeva M, Strokin M, Wang H, Ubl JJ & Reiser G (2003). Arachidonic acid in astrocytes blocks Ca^{2+} oscillations by inhibiting store-operated Ca^{2+} entry, and causes delayed Ca^{2+} influx. *Cell Calcium* **33**, 283–282.

Smith JS, Imagawa T, Ma J, Fill M, Campbell KP & Coronado R (1988). Purified ryanodine receptor from rabbit skeletal muscle is the calcium release channel of sarcoplasmic reticulum. *J General Physiol* **92**, 1–26.

Somlyo AV & Franzini-Armstrong C (1985). New views of smooth muscle structure using freezing, deep-etching and rotary shadowing. *Experientia* **41**, 841–856.

Tang J, Lin Y, Zhang Z, Tikunova S, Birnbaumer L & Zhu MX (2001). Identification of common binding sites for calmodulin and inositol 1,4,5-trisphosphate receptors on the carboxyl termini of trp channels. *J Biol Chem* **276**, 21303–21310.

Trepakova ES, Csutora P, Hunton DL, Marchase RB, Cohen RA & Bolotina VM (2000). Calcium influx factor directly activates store-operated cation channels in vascular smooth muscle cells. *J Biol Chem* **275**, 26158–26163.

Treves S, Franzini-Armstrong C, Moccagatta L, Arnoult C, Grasso C, Schrum A, Ducreux S, Zhu MX, Mikoshiba K, Girard T, Smida-Rezgui S, Ronjat M & Zorzato F (2004). Junctate is a key element in calcium entry induced by activation of InsP3 receptors and/or calcium store depletion. *J Cell Biol* **166**, 537–548.

Van Breemen C, Chen Q & Laher I (1995). Superficial buffer barrier function of smooth muscle sarcoplasmic reticulum. *Trends Pharmacol Sci* **16**, 98–105.

Venkatachalam K, van Rossum DB, Patterson RL, Ma H-T & Gill DL (2002). The sellular and molecular basis of store-operated calcium entry. *Nature Cell Biol* **4**, E263–E272.

Vorndran C, Minta A & Poenie M (1995). New fluorescent calcium indicators designed for cytosolic retention or measuring calcium near membranes. *Biophys J* **69**, 2112–2124.

Watanabe H & Burnstock G (1976). Junction subsurface organs in frog sympathetic ganglion cells. *J Neurocytol* **5**, 125–136.

Xu S-Z & Beech DJ (2001). TRPC1 is a membrane-spanning subunit of store-operated Ca^{2+} channels in native vascular smooth muscle cells. *Circ Res* **88**, 84–87.

Yagodin S, Holtzclaw LA & Russell JT (1995). Subcellular calcium oscillators and calcium influx support agonist-induced calcium waves in cultured astrocytes. *Mol Cell Biochem* **149/150**, 137–144.

Yuan JP, Kiselyov K, Shin DM, Chen J, Shcheynikov N, Kang SH, Dehoff MH, Schwarz MK, Seeburg PH, Muallem S & Worley PF (2003). Homer binds TRPC family channels and is required for gating of TRPC1 by IP3 receptors. *Cell* **114**, 777–789.

Acknowledgements

I thank M. P. Blaustein for insightful discussion and support, D. L. Gill, and M. Juhaszova for comments on the manuscript and E. Carafoli, G. Krapivinsky, R. J. Wojcikiewicz and F. Wuytak for generous gifts of antisera. Supported by NIH grant NS-048263, a Grant-in-Aid from the American Heart Association Mid-Atlantic Affiliate, the Alzheimer's Association grant IIRG-03-5665, funds from the University of Maryland School of Medicine, and by NIH grant NS-16106 (to M.P. Blaustein).